RSC Advances

PAPER

View Article Online
View Journal | View Issue

Cite this: *RSC Adv.*, 2023, **13**, 32083

An economical and simple method for preparing highly permeable and chlorine-resistant reverse osmosis membranes with potential commercial applications†

Junqing Sun,[a] Qianwen Zhang,[b] Wenjing Xue,[a] Wande Ding, *[ac] Kefeng Zhang[a] and Shan Wang*[a]

The improvement in the overall efficiency of thin-film composite (TFC) reverse osmosis (RO) membranes is limited by their low permeability and sensitivity to degradation by chlorine. In the present study, polypiperazine (PIP), the commonly used amine monomer in preparing commercial TFC nanofiltration (NF) membranes, was used to regulate the *m*-phenylenediamine (MPD) based interfacial polymerization (IP) process. The results showed that addition of PIP optimized the micro-structure and surface properties of the polyamide (PA) layer. When the MPD and PIP mass ratio was 1 : 1, the $TFC_{W\text{-}1:1}$ membrane exhibited 70% flux enhancement compared to pure MPD-based $TFC_{W\text{-}1:0}$ membranes. Besides, the $TFC_{W\text{-}1:1}$ membrane exhibited better chlorine-resistant performance since the NaCl rejection declined to just 3.8% while it was 11.3% for $TFC_{W\text{-}1:0}$ membranes after immersion in 500 ppm NaClO solution for 48 h. Such improvement can be attributed to the increased number of unreacted amine groups and the thickness of the PA layer that PIP brought, which provided a sacrificial protective layer to consume the active chlorine, and thus maintain the integrity of the inner rejection layer. In all, the novelty and purpose of the present work is to find a more simple and scalable method to fabricate high-performance TFC RO membranes by using commonly, cheaply and frequently used materials.

Received 4th September 2023
Accepted 26th October 2023

DOI: 10.1039/d3ra06015b

rsc.li/rsc-advances

Introduction

Membrane separation technology, especially for reverse osmosis (RO) desalination, has become a promising method in addressing water shortages around the world due to its simple operation and high efficiency as well as the smaller footprint.[1,2] As the heart of RO, a high-performance membrane plays the most important role in determining the separation efficiency. Currently, thin film composite membranes (TFC) are the commonly used type of commercial RO membrane because of their reasonable water flux and superior rejection for monovalent ions. This type of membrane is generally synthesized *via* the interfacial polymerization (IP) method, in which a dense polyamide layer (PA) is constructed on the porous ultrafiltration support through the reaction between *m*-phenylenediamine (MPD) and trimesoyl chloride (TMC).[3,4] To date, continuous effort has been devoted by researchers to the improvement of membrane properties to promote their further development, and RO technology has already been widely applied in the fields of brackish water desalination, seawater desalination and wastewater reuse, *etc*.[5,6]

TFC membranes have dominated the RO membrane market for decades, however, their disadvantages have gradually become apparent meanwhile. One of the basic limitations is the 'trade-off' effect between selectivity and permeability.[7] To break this inherent limitation, scientists have developed many approaches to prepare high-performance RO membranes with both high water permeability and high salt selectivity, which can be classed into three categories: (1) manipulating IP parameters, such as using novel reaction monomer and adjusting IP reaction conditions; (2) incorporating nanomaterial within PA layer in improving membrane properties and constructing nanochannel; and (3) constructing intermediate layer and regulate the PA layer structure by using its domain limiting effect.[8,9] Li *et al.* designed and synthesized a novel amine monomer (4-morpholinobenzene-1,3-diamine (MpMPD)) with a morpholine group, and then it was reacted with TMC to prepare the PA layer. The zwitterionic surface and thinner thickness of the PA layer contributed to 24% flux enhancement with relatively high (97.8%) NaCl rejection compared to the MPD-based TFC membranes.[10] Besides, since the first literature of thin film nanocomposite membrane (TFN)

[a]*School of Municipal and Environmental Engineering, Shandong Jianzhu University, Jinan, 250101, China. E-mail: dingwande18@sdjzu.edu.cn; sg073ws@163.com*
[b]*School of Environment, Tsinghua University, Beijing, 100084, China*
[c]*Shandong Shuifa Environmental Technology Co., Ltd, Jining, 272000, China*

† Electronic supplementary information (ESI) available. See DOI: https://doi.org/10.1039/d3ra06015b

published by Hoek *et al.*,[11] in which zeolite nanoparticles were introduced in the PA layer, various types of nanomaterials (*e.g.* SiO_2, TiO_2, carbon nanotube (CNT), graphene oxide (GO), metal–organic frameworks (MOFs)) were gradually applied in the fabrication of polyamide membranes with specific properties, such as high permeability and selectivity, antifouling and antibacterial capacity.[12] Liu *et al.* loaded 2D-MOF nanosheets in the TFC membrane rejection layer, and the improved hydrophilicity and extra water channel induced 250% flux enhancement with 99.2% NaCl rejection of the TFN membranes. Meanwhile, 96.9% flux recovery ratio after the humic acid (HA) pollution implied the achievement of an outstanding antifouling property of the modified TFN membranes.[1] Furthermore, based on the spatial shielding effect and interaction with MPD molecules, Zhao *et al.* constructed a multifunctional crown ether interlayer on the ultrafiltration membrane for the purpose of reducing the diffusion of amines to the water-oil reaction interface. Resultingly, a thinner PA layer (~50 nm) with a uniform and regular morphology was achieved. The change of PA layer structure resulted in a 3.64 times higher water flux accompanied by a satisfied NaCl rejection compared to pristine TFC membrane.[4] All the three modification methods possessed the potential in breaking the 'trade-off' effect, which provided a broad choice in preparing highly permeable and selective RO membranes.

Another basic limitation of TFC membranes was the chlorine-instability during the RO process. Generally, the amide bond is the most important group in the PA layer, which determines the separation performance of TFC membranes. However, it was easily attacked by active chlorine through the reversible *N*-chlorination on the amide bond (N–H) and the irreversible aromatic ring-chlorination *via* Orton rearrangement, which would destroy the integrity of the rejection layer and deteriorate the membrane separation performance.[13–15] Based on the methods of improving the membrane permeability, chlorine-resistant TFC membranes can also be obtained meanwhile. Yu *et al.* synthesized TFC RO membranes by using two novel reaction monomers of *m*-phenylenediamine-4-methyl (MMPD) in aqueous phase and cyclohexane-1,3,5-tricarbonyl chloride (HTC) in organic phase. Except for the better permeability about 53.0 L m^{-2} h^{-1} compared to commercial MPD-based polyamide membrane, an excellent chlorine-resistance performance was also investigated under 3000 ppm h Cl, which was mainly ascribed to the reduced probability of *N*-chlorination and Orton-rearrangement by using monomer MMPD.[16] Li *et al.* introduced 4,40-((5-(chlorocarbonyl)-1,3-phenylene) bis(thiodiyl))dibenzoyl chloride (T-TDC) in the TMC organic phase and reacted with MPD to prepare TFC membranes. They were satisfied to find that the rejection of the membrane with T-TDC were all much larger than MPD/TMC-based polyamide membrane after the chlorination test, suggesting that the introduction of thioether groups provided effective chlorine capture for avoiding the attacking of amide bonds from being chlorinated.[13] Furthermore, Asempour. *et al.* grafted halloysite nanotubes (HNTs) with poly(amidoamine) PAMAM dendrimers and then were incorporated in the PA layer. The improved properties of membrane surface, extra water channel as well as the extra amine and amide groups supplied by the PAMAM functionalized HNTs made a contribution to not only the doubled water flux, but also a higher chlorination-resistance of the TFN membranes, since no statistically significant change was detected in terms of the salt rejection and water flux under the chlorine exposure of 12 000 ppm h.[17] Similarly, Chae *et al.* fabricated TFN membranes by incorporating GO in the PA layer, and the maintained NaCl rejection of the TFN membranes suggested the better chlorine-resistant compared to the pristine TFC membrane, which resulted from the formation of hydrogen bonding between amide bond and GO that hindered the attack of chlorine to the amidic hydrogen (*i.e.*, the first step of the chlorination process).[18]

As discussed above, various modification methods have been extensively explored by researchers in improving the performance (separation performance, antifouling performance, antibacterial performance and chlorine-resistant performance) of TFC membranes up to now. Among them, using two kinds of amine monomers to tailor the structure of PA layer and providing extra reaction site for active chlorine in improving both separation performance and chlorine-resistance of the MPD/TMC-based TFC membranes are believed to possess the most potential value on the industrial-scale membrane production because of its excellent compatibility.[19,20] Compared to other novel amine monomers, piperazine (PIP) was a simple heterocyclic amine molecule, which is the most commonly used monomer in preparing TFC NF membranes and exhibited a much loosen PA structure compared to MPD/TMC-based TFC RO membranes, thus inducing higher water flux but relative low rejection for NaCl.[9,21] Besides, PIP-based polyamide membranes consist of tertiary amide linkages together with nonaromatic, aliphatic diamines, which are believed to provide favorable resistance towards *N*- and ring-chlorination and hence improve the chlorine-resistant of TFC membranes.[22] These features of PIP monomer well match the requirement of the strategy in regulating the membrane properties by mixing PIP and MPD as aqueous phase, which may develop a simpler and cheaper method in constructing high-performance (better permeability with excellent rejection for NaCl, better chlorine-resistant) RO membranes. However, no systematic study was performed to prove this.

Therefore, in this work, MPD and PIP mixture in the aqueous phase was used for providing the amine monomers to react with TMC in the organic phase, and the relationships between membrane property and the ratio of MPD and PIP were investigated thoroughly, which was tended to analyze the influence of PIP on the structure and properties of the PA layer. By using XPS, SEM, AFM and contact angle *e.g.*, the change of membrane morphology, hydrophilicity, roughness and functional groups induced by PIP was determined. Besides, the effect of PIP on the separation performance and chlorine-resistant performance of the TFC membranes was also evaluated. The novelty and purpose of the present work is to find a more simple and scalable method to fabricate high-performance TFC RO membranes by using commonly, cheaply and frequently used materials.

Materials and methods

Materials

Polysulfone ultrafiltration membrane (PS, M_w = 50 000 Da) was purchased from Beijing Originwater Technology Co., Ltd (China).

Morphenediamine (MPD, 99.5%), piperazine (PIP, 99%), trimesoyl chloride (TMC, 98%) and isopropyl alcohol (99.7%) were obtained from Shanghai Aladdin Reagent Co., Ltd (China). Sodium hypochlorite (NaClO, 4.0%) and sodium dodecyl sulfate (SDS, 99%) were supplied by Shanghai Maclin Biochemical Technology Co., Ltd (China). Hexane (98%), and NaCl (99%) were provided by Shanghai Sinopharm Chemical Reagent Co., Ltd (China). All chemical reagents were used without further treatment and deionized (DI) water was used throughout the experimental study.

Preparation of the TFC membranes

Before the formation of TFC membranes, PS ultrafiltration membrane was first treated by 50% isopropyl alcohol solution for 6 h. Then, the MPD/PIP-TMC TFC membranes were prepared through the IP method by adjusting the monomer composition of aqueous phase. Briefly, aqueous phase solution containing 2 wt% MPD/PIP mixed monomer and 0.15 wt% SDS were poured on the top surface of PS substrate and maintained the immersion for 120 seconds. The MPD and PIP mass ratio was specifically divided into 1 : 0, 4 : 1, 2 : 1, 1 : 1, 1 : 2, 1 : 4 and 0 : 1. After removing the excess solution using N_2, the amine monomer contained surface of the PS substrate was then immersed in 0.1 w/v% TMC–*n*-hexane solution to continue the IP process for 60 seconds. Finally, the resultant membrane was washed thoroughly with *n*-hexane and heat-treated for 5 min at 80 °C. Fig. 1 illustrated the preparation procedure of TFC membranes and the different membranes were denoted as $TFC_{W\text{-}1:0}$, $TFC_{W\text{-}4:1}$, $TFC_{W\text{-}2:1}$, $TFC_{W\text{-}1:1}$, $TFC_{W\text{-}1:2}$, $TFC_{W\text{-}1:4}$ and $TFC_{W\text{-}0:1}$, respectively.

Characterization

Prior to the characterization, all the membranes were oven-dried overnight at 50 °C. Surface functional groups of the TFC membranes were determined by the Fourier transform infrared (FTIR) equipped with attenuated total reflection (ATR) stage (Tensor 27, Bruker, Germany). In order to confirm the element composition of the PA layer, X-ray photoelectron spectrometer (XPS, ESCALAB 250Xi, Thermo Scientific, USA) was used. By peak fitting of different chemical elements, specific functional groups with accurate content percentages can be obtained. Besides, cross-linking degree (D) was an important parameter in analyzing the separation performance, and it can be calculated according to the oxygen and nitrogen atomic ratio ($R_{O/N}$) as the following equations:[1,2]

$$R_{O/N} = \frac{4N + 3M}{2N + 3M} \quad (1)$$

$$\text{Cross-linking degree}(D) = \frac{M}{M + N} \times 100\% \quad (2)$$

where N was on behalf of the percent of linear structure and M represent the percent of the network cross-linked structure in the PA layer, respectively.

Scanning electron microscopy (SEM, GeminiSEM 300, Zeiss, Germany) was used to observe the surface morphology and cross-section structure of the PA layer. For the cross-section samples, the nonwoven fabrics of the membrane were first manually peeled off from the back side. After that, the membrane was frozen in liquid nitrogen and then cracked quickly. It was worth noting that all samples were gold-sputtered for 120 s to enhance their conductivity prior to the SEM investigation. To determine the accurate thickness of the PA layer, the membrane samples were embedded in epoxy resin and the resin capsules were subjected to curing at 60 °C for 24 h. Then, approximately 60 nm thick sections were sectioned by an ultramicrotome (EM UC7, Leica, Germany) with a diamond knife and transferred to copper grids for transmission electron microscope (TEM, Thermo Fisher, Talos F200S G2, USA) observation. By using *in situ* atomic force microscopy (AFM, Dimension Icon, Bruker, Germany), surface roughness (defined by three parameters R_a, R_q, R_z) and specific surface morphology can be confirmed. The surface hydrophilicity reflected by the contact angles can be measured through a contact angle meter (DSA100, Kruss, Germany). Each sample measurement was repeated for three times to obtain the average contact angle value. Membrane potential was characterized by a solid surface

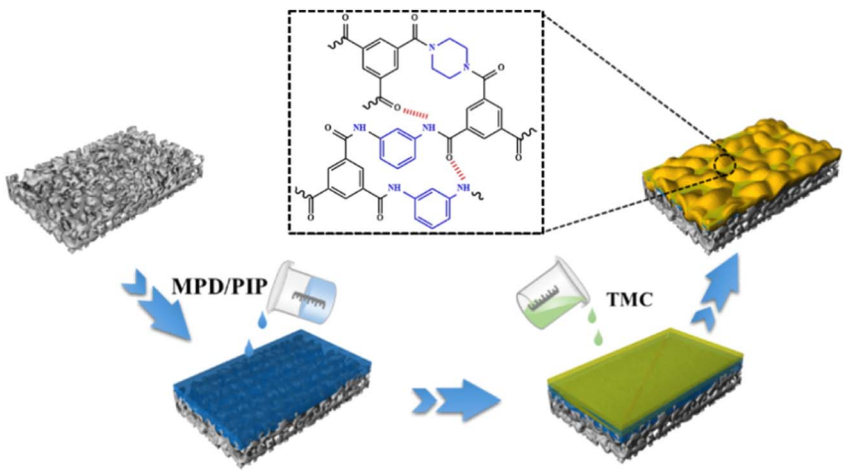

Fig. 1 The preparation procedure of TFC membranes.

potential analyzer (Surpass3, Anton Paar, Austria) at the pH ranging from 2 to 10.

The diffusion rate of MPD and PIP monomers into the organic phase was measured by the following procedure.[23] First, 50 mL of 2.0 wt% MPD/PIP mixed solution (MPD/PIP mass ration ranging from 1 : 0 to 0 : 1) was poured into a 250 mL beaker, and 50 mL of 0.15 wt% TMC/*n*-hexane was carefully injected into the aqueous phase. After 60 s duration, 3 mL of water containing MPD/PIP was removed from the aqueous and organic interface and placed in quartz cuvettes. The diffusion rate of PIP from the aqueous phase to the interface was studied using a UV-vis spectrophotometer (Specord 200 Plus, Analytikjena, Germany). For the two monomers MPD and PIP, the absorption peaks at 320 nm and 247 nm were selected to calculate the diffusion concentration of the aqueous monomer per unit time, that is, the diffusion rate of the mixed monomer (Fig. S1†).

By using stopped-flow mass spectrometry (SFMS) (SX20, Applied Photophysics), the effect of PIP concentration on the reaction rate between aqueous phase and organic phase was studied.[24] Briefly, aqueous phase and organic phase are rapidly mixed together and then 'stopped' in an observation cell. The sample cell is irradiated with monochromatic light and as the reaction proceeds the change in the recorded signal, usually a fluorescence signal or absorbance at a specific wavelength, is recorded as a function of time. Finally, the reaction rate can be determined by analyzing the generated kinetic transients.

Separation performance of TFC membranes

The water flux and salt rejection of TFC membranes were tested using RO evaluation equipment (FlowMen-0021-HP, China, as shown in Fig. S2†) with three 24 cm^2 parallel filtration cells. 2000 ppm NaCl and Na_2SO_4 solution were used as the feed solution to evaluate the rejection of the TFC membrane for monovalent and divalent ions, respectively. Before the collection of filtration data at 16 bar, TFC membranes should be pre-compressed under 18 bar for at least 0.5 h to achieve a stable water permeance. The specific calculation formulas of water flux (J, L m^{-2} h^{-1}), water permeability (A, L m^{-2} h bar), salt rejection (R, %) and separation selectivity (α) of NaCl to Na_2SO_4 of the TFC membranes were as follows:[24,25]

$$J = \frac{\Delta V}{A_m \cdot \Delta t} \quad (3)$$

$$A = \frac{J}{\Delta P - \Delta\pi} \quad (4)$$

$$R = 1 - \frac{C_p}{C_f} \quad (5)$$

$$\alpha = 1 - \frac{R_{NaCl}}{R_{Na_2SO_4}} \quad (6)$$

where ΔV (L) is the permeated water volume over the measuring time interval of Δt, A_m (m^2) is the effective membrane area, C_p (g L^{-1}) is the permeate salt concentration, C_f (g L^{-1}) is the feed solution concentration, ΔP (bar) is the transmembrane pressure, $\Delta\pi$ (bar) is the osmotic pressure of the feed solution, respectively.

Chlorine-resistant performance of the TFC membranes

The chlorine-resistant property evaluation was conducted under a static chlorination test. Briefly, the TFC membranes were immersed in 500 ppm NaClO solution for 12 h, 24 h and 48 h to conduct the chlorination process. After that, all the chlorinated membranes were rinsed thoroughly and then stored in DI water for 48 h. Finally, the stabilized water flux and salt rejection of the chlorinated TFC membranes were re-evaluated by the RO filtration unit and then the effect of PIP on the chlorine-resistant performance of the TFC membranes could be analyzed.

Results and discussion

Surface functional groups, diffusion rate of mixed amine and IP reaction rate of TFCW membranes

Surface functional groups of TFC_W membranes were detected by ATR-FTIR analysis. In Fig. 2a, $TFC_{W\text{-}1:0}$ membranes showed characteristic peaks at 1663 cm^{-1}, 1604 cm^{-1} and 1546 cm^{-1}, which was corresponding to the C=O stretching vibration of amide I band, C=C ring stretching vibration of aromatic amide band and N–H in-plane flexural vibration of amide II band, indicating the successful construction of the aromatic PA layer on the ultrafiltration membrane.[26,27] After addition of PIP, the peak intensity at 1663 cm^{-1} and 1546 cm^{-1} gradually declined with the increased loading concentration of PIP till completely disappeared for the $TFC_{W\text{-}0:1}$ membrane. Furthermore, the peak at 1604 cm^{-1} happened to blue shift to 1620 cm^{-1}, and above changes suggested the transformation of the PA layer from 'fully-aromatic' PA structure to 'semi-aromatic' PA structure.[28] Besides, the peak at 1443 cm^{-1} was detected in all membranes, which was mainly attributed to the O–H vibration that originated from the hydrolysis of the unreacted acyl chlorides in the PA layer.[29]

Fig. 2b displayed the diffusion rate of the mixed amine from the aqueous solution to the organic phase. As for pure MPD, the diffusion rate was very fast, which would result in the fast formation of the initial dense PA layer and hinder the further penetration of MPD molecules to the organic phase.[30] With the loading concentration of PIP increased, the diffusion rate of MPD toward the organic phase gradually declined while the diffusion rate of PIP enhanced. Generally, the reaction between MPD or PIP and TMC in a same system kept a competitive relationship, and would lead to a different PA structure. It was seen that before the 1 : 1 mass ratio between MPD and PIP, the diffusion rate of MPD was always higher than that of PIP, indicating MPD molecules run faster to the interface of aqueous solution and organic phase. At this time, the IP process was believed dominated by the reaction between MPD and TMC. When further increased PIP content surpassed MPD/PIP mass ratio about 1 : 1, the diffusion rate of PIP gradually exceeded MPD. We speculated that PIP would gradually replace the dominant position of MPD to react with TMC, and more PIP

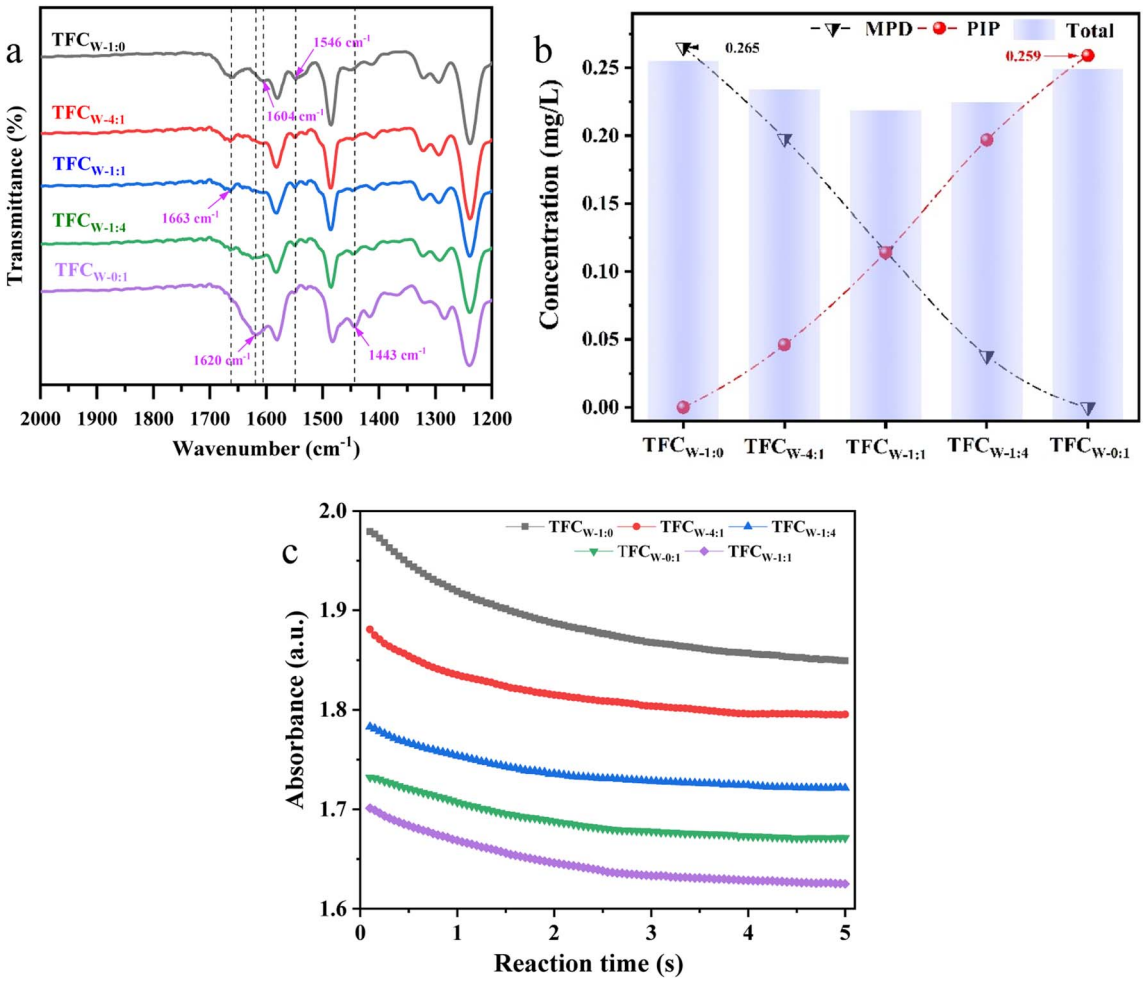

Fig. 2 (a) ATR-FTIR spectra of TFC$_W$ membranes, (b) diffusion rate of mixed amine from aqueous phase to the organic phase, and (c) IP reaction rate of mixed amine and TMC.

molecules would participate in the IP process with the increased loading concentration. These changes could help to change the reaction rate of IP process and further control the morphology and performance of PA films.[31]

In order to further understand the effect of PIP on constructing PA active layer, IP reaction rate between aqueous phase containing mixed amines and organic phase was monitored using SFMS, and the results were shown in Fig. 2c. Obviously, the fastest reaction rate reflected by the higher signal strength of PA was induced by the reaction between MPD and TMC, which could contribute a greater amount of PA in unit time. With the introduction of PIP, the signal strength of PA gradually decreased, implying that PIP lowered the total reaction rate of the IP process compared to MPD in unit time. Of note, the TFC$_{W-1:1}$ membrane exhibited the lowest reaction rate for the most likely reason of the lowest total diffusion rate of mixed amine as proved in Fig. 2b. Furthermore, it was seen that IP reaction achieved equilibrium in a very short time since the absorbance of PA became stable after 4 s. Extension of reaction time gradually brought decline of the reaction rate, which further provided the evidence of the self-termination effect of the IP.[32] As a result, the reaction rate between amine monomers and TMC could be mitigated by the addition of PIP, which would ultimately affect the membrane structure and properties of the resultant membrane.

Morphological characterizations of the TFCW membranes

Surface morphology and roughness of TFC$_w$ membranes were investigated by SEM and AFM as presented in Fig. 3 and the 3D AFM images were shown in Fig. S3.† For TFC$_{W-1:0}$ membranes, it showed the typical "ridge-valley" structure with a mean roughness about 112.00 nm induced by the conventional IP methods on the top of ultrafiltration support.[33] Furthermore, the "ridge-valley" structure became smaller and transformed into a ring structure accompanied by a smoother membrane surface with the introduction of PIP in aqueous phase (Fig. 3b–g). When MPD/PIP mass ratio was 4 : 1, a small and uniform ring structure presented on the TFC$_{W-4:1}$ membrane surface and its surface roughness was 69.8 nm as summarized in Table 1. As the increment of PIP concentration, the ring structure became much clearer with the enlarged ring size. Till the MPD/PIP mass ratio reached 0 : 1, more flat and incomplete ring structure

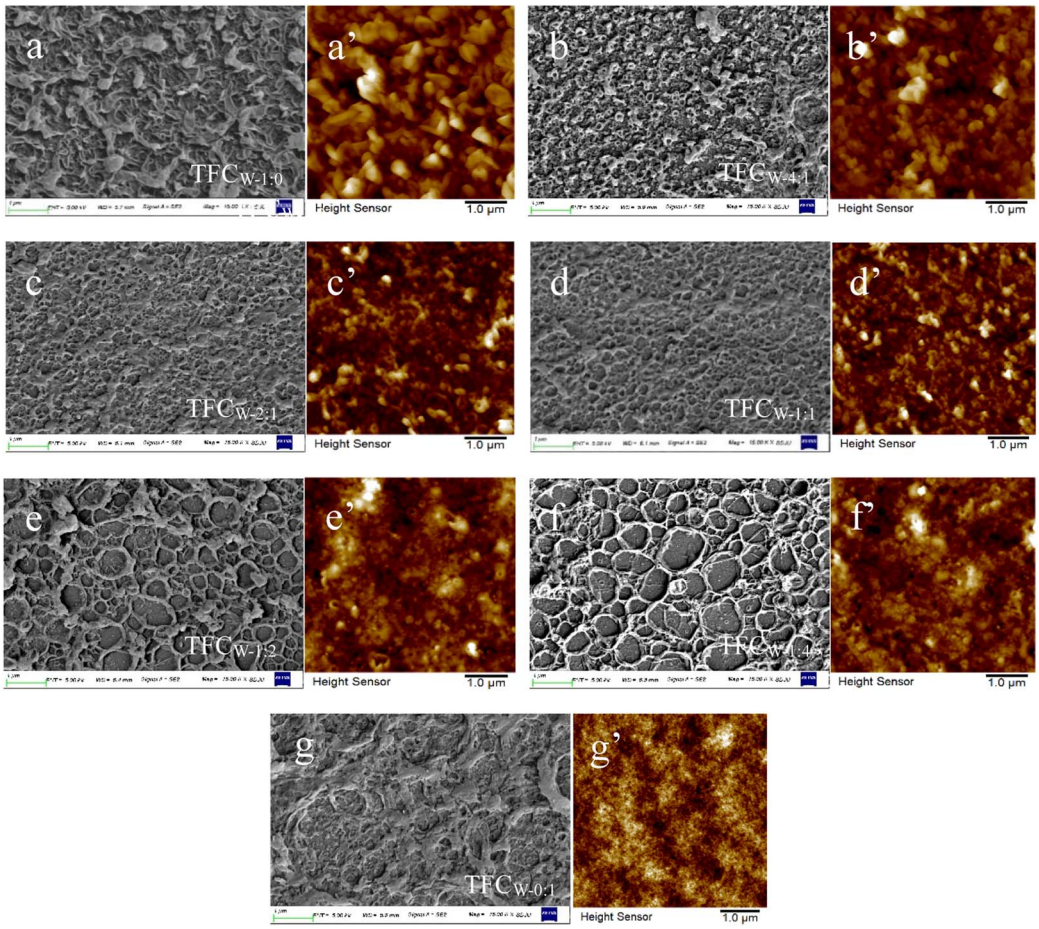

Fig. 3 Surface morphology and roughness of TFCw membranes under different loading content of PIP in aqueous phase.

occurred on the $TFC_{W\text{-}0:1}$ membrane surface. Table 1 summarized the surface roughness parameter of TFC_W membranes, in which it showed a decreased trend in surface roughness for the TFC_W membranes, which was in accordance with the membrane morphology.

Fig. 4 presented the corresponding cross-section images of $TFC_{W\text{-}1:0}$, $TFC_{W\text{-}1:1}$ and $TFC_{W\text{-}0:1}$ membrane through SEM and TEM. It was obvious that the membrane consisted of a dense PA layer and a porous support layer. After the addition of PIP, the thickness of the PA layer was visibly increased (Fig. 4b and c). Based on the TEM images, the thickness of the PA layer for

Table 1 The surface roughness parameter of the TFC_W membranes

	Surface roughness parameter		
TFC_W	R_q (nm)	R_a (nm)	R_z (nm)
$TFC_{W\text{-}1:0}$	112.00	89.90	855.00
$TFC_{W\text{-}4:1}$	69.80	51.80	554.00
$TFC_{W\text{-}2:1}$	30.50	23.70	217.00
$TFC_{W\text{-}1:1}$	25.60	19.60	213.00
$TFC_{W\text{-}1:2}$	19.00	14.40	176.00
$TFC_{W\text{-}1:4}$	17.50	13.30	202.00
$TFC_{W\text{-}0:1}$	5.77	4.63	52.40

$TFC_{W\text{-}1:0}$, $TFC_{W\text{-}1:1}$ and $TFC_{W\text{-}0:1}$ membrane can be accurately measured as 194.8 nm, 267.8 nm and 592.7 nm, respectively. The structure change for both membrane surface and cross-section was mainly attributed to the formation mechanism of the PA layer through IP on the membrane surface. Generally, amine monomers in aqueous were first diffused across the water–oil interface and underwent polycondensation with acyl chloride monomer in organic phase, named as the fast incipient film formation, followed by the film growth controlled by the diffusion of amines across the initially-formed film.[34] For $TFC_{W\text{-}1:0}$ membrane, the fastest diffusion of MPD leads to the rapid formation of a highly cross-linked, dense incipient layer, which would greatly inhibit the MPD diffusion and film growth, resulting in the rougher and thinner PA layer as displayed in Fig. 5a. However, when mixed MPD solution with PIP, the IP process was greatly interfered due to the lower diffusion of amine monomers, lower reaction rate of aqueous phase and organic and lower activity of PIP compared to MPD, which induced a relatively loosen incipient film. The structure change provided the opportunity to allow more MPD and PIP molecules to transport across the incipient film and penetrate deeply into the organic phase to react with TMC, which was then adhered to the basal PA layer and made the PA layer change from rough to relatively flat

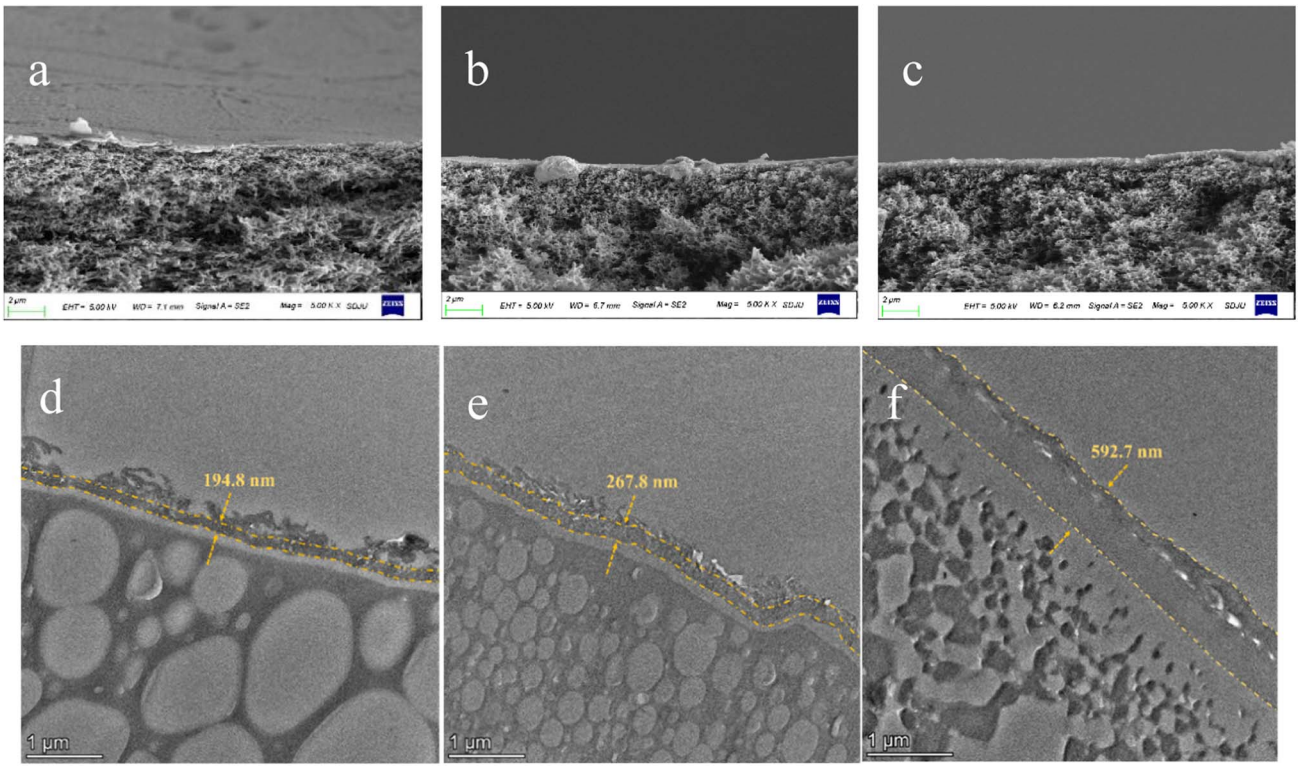

Fig. 4 Cross-sectional images of $TFC_{W\text{-}1:0}$ (a) and (d), $TFC_{W\text{-}1:1}$ (b) and (e) and $TFC_{W\text{-}0:1}$ (c) and (f) membranes detected by SEM and TEM.

structure as illustrated in Fig. 5b.[35] Furthermore, the increased PIP concentration gradually allowed more amine monomers to combine with the TMC through the initial sparse amide layer, which led to the formation of the obvious ring structure. Especially for the TFC_W membrane that PIP content surpassed 50%, the incipient film was gradually dominated by the reaction between PIP and TMC, and more loosen incipient film was constructed compared to that dominated by MPD. Resultingly, more penetrated PIP molecules participate in the expanded IP process, thus the thickness of PA layer further increased as exhibited in Fig. 5c.

Surface element composition of TFCW membranes

XPS measurement was further used to determine the element composition and the cross-linking degree of PA layer. Three peaks belonging to C 1s, N 1s and O 1s were detected at 284.8 eV, 400.0 eV and 531.0 eV as displayed in Fig. 6a, and the relative content was summarized in Table 2. Through the calculation, $TFC_{W\text{-}1:0}$ membrane showed the highest cross-linking degree about 0.96, indicating the formation of a denser rejection layer that composed of an amount of network cross-linking structure ($R_{O/N} = 1.03$). For the TFC_W membrane prepared by the mixed amine (MPD/PIP) and TMC, due to the

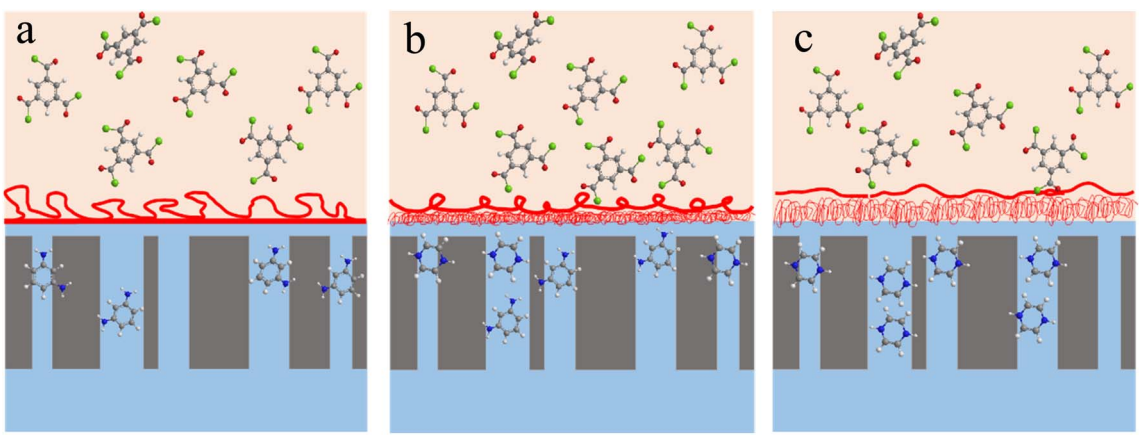

Fig. 5 Formation mechanism of the PA layer of $TFC_{W\text{-}1:0}$ membrane (a), $TFC_{W\text{-}4:1}$ membrane (b) and $TFC_{W\text{-}1:4}$ membrane (c) through IP method.

participation of PIP in the reaction with TMC, the PA layer gradually composited of both 'fully-aromatic' structure and 'semi-aromatic' structure, and the network cross-linking structure occurred to be replaced by part linear structure.[36,37] $TFC_{W\text{-}1:1}$ membrane exhibited the lowest cross-linking degree that was related to the lowest diffusion rate of amine in aqueous phase toward organic phases and the lowest reaction rate of IP. However, it was noticed that when the concentration of PIP exceeded 50%, the cross-linking degree began to increase. This can be explained by the following: (1) increased diffusion rate of mixed amine towards reaction interface accelerates the IP reaction rate; (2) when the content of PIP was higher than MPD, the reaction between PIP and TMC gradually controlled the IP process, and the initial PA layer would become more loosen than that formed by MPD and TMC. Consequently, more amine molecules penetrated through the initial PA layer and reacted with TMC, and hence contributed to the increased cross-linking degree.

The content of carboxyl group in the PA layer originated from the hydrolyzation of the unreacted acyl chloride groups was another important parameter in determining the membrane surface hydrophilicity. To quantitatively evaluate the contents of carboxyl group on the membrane surfaces, the O 1s of the TFC_W membranes were decomposed into three peaks at ~531.1 eV, ~532.1 eV, ~533.5 eV, which was corresponding to N–C═O*/O–C═O*, H–*O–C/C–*O–C and O═C–*O groups,[28] as presented in Fig. 6. In detail, the content of carboxyl group was 13.2% for $TFC_{W\text{-}1:0}$ membrane, 16.8% for $TFC_{W\text{-}4:1}$ membrane, 20.1% for $TFC_{W\text{-}1:1}$ membrane, 15.6% for $TFC_{W\text{-}1:4}$ membrane and 10.1% for $TFC_{W\text{-}0:1}$ membrane, respectively. Generally, the higher carboxyl group content the membrane surface possessed, the better hydrophilicity the membrane surface was, which was believed to benefit for the membrane permeability. It should be mentioned that the core-level C 1s after deconvolution and the corresponding chemical species in the nanofilm were displayed and summarized in Fig. S4 and Table S1.†

Table 2 Surface element composition of TFC_W membranes

Membrane	C (at%)	N (at%)	O (at%)	O/N	*D* (%)
$TFC_{W\text{-}1:0}$	72.12	13.75	14.12	1.03	0.96
$TFC_{W\text{-}4:1}$	71.40	13.21	15.39	1.17	0.77
$TFC_{W\text{-}1:1}$	71.90	12.84	15.26	1.19	0.74
$TFC_{W\text{-}1:4}$	70.62	13.85	15.52	1.12	0.83
$TFC_{W\text{-}0:1}$	71.18	13.77	15.05	1.09	0.87

The content of the unreacted amine (–NH, $–NH_2$, $–NH_2^+$ and $–NH_3^+$) in the PA layer played a significant role in providing extra sites to react with the active Cl, which may decrease the direct attack of active Cl to amide group and thus maintain the membrane integrity.[38] Through the peak fitting of N 1s in TFC_W membranes, the N-related peaks were detected at 400.0 eV, 389.9 eV and 401.3 eV, which belonged to the O═C–NH group, C–NH/C–NH_2 group and C–NH_2^+/C–NH_3^+ group as illustrated in Fig. 7. The content percentage of O═C–NH groups matched the changing trend with the cross-linking degree of the TFC_W membranes. For the TFC_W membranes based on the introduction of PIP, the loose PA layer allowed more amines to diffuse through the crosslinked structure of the nanofilm formed at the interface,

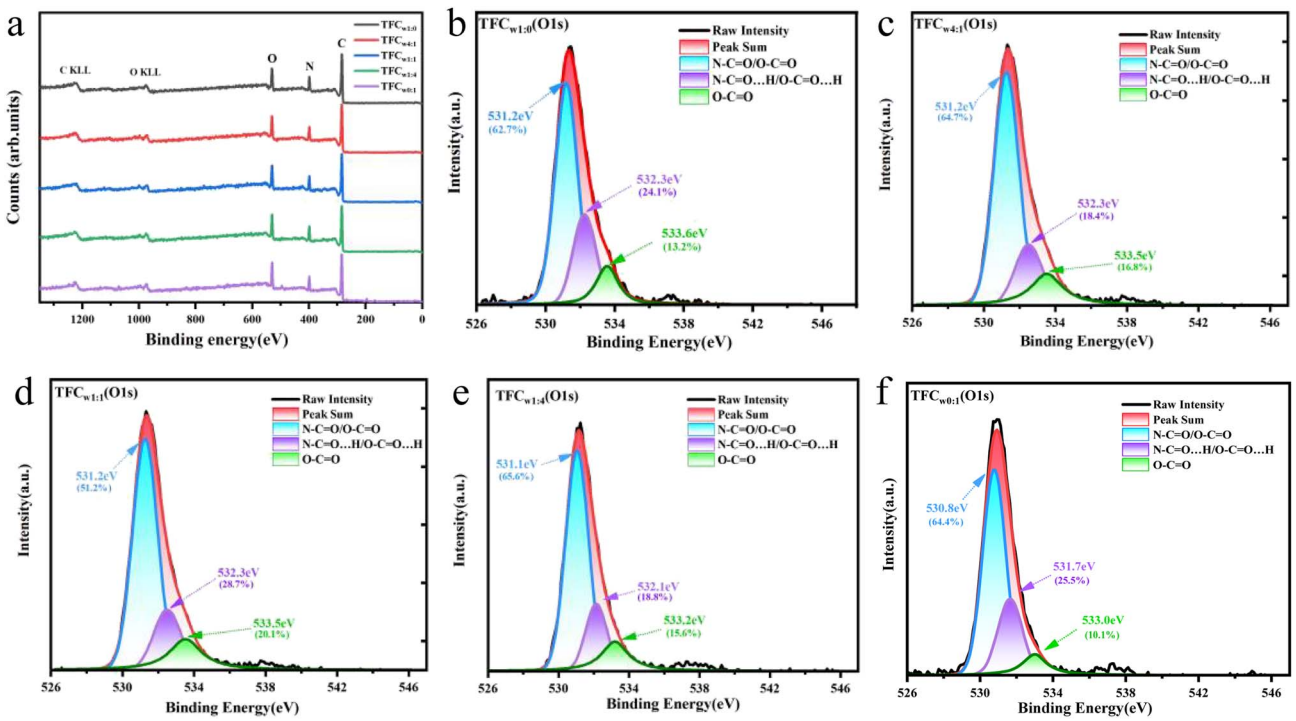

Fig. 6 XPS spectra of all the TFC_W membranes (a), O 1s deconvoluted peaks in XPS spectra of $TFC_{W\text{-}1:0}$ membrane (b), $TFC_{W\text{-}4:1}$ membrane (c), $TFC_{W\text{-}1:1}$ membrane (d), $TFC_{W\text{-}1:4}$ membrane (e) and $TFC_{W\text{-}0:1}$ membrane (f).

and hence remained partially unreacted amine inside or on the surface of the nanofilm.[28] Specifically, the total percentage of unreacted amine were 19.7%, 23.4%, 25.2%, 24.8% and 22.9% for $TFC_{W\text{-}1:0}$, $TFC_{W\text{-}4:1}$, $TFC_{W\text{-}1:1}$, $TFC_{W\text{-}1:4}$ and $TFC_{W\text{-}0:1}$ membrane, respectively. Similarly, when the PIP loading concentration surpassed 50%, the increased cross-linking degree indicated the more consumption of amine group, and hence decreased the unreacted amine content in the membrane. The lowest content of the unreacted amine was detected in $TFC_{W\text{-}1:0}$ membrane, which was mainly caused by the fast reaction rate and the reaction rate of IP process between TMC and MPD, and hence led to the highest cross-linking degree.

Contact angle and membrane potential of TFCW membranes

The surface charge was a key parameter in separating different salt solutions. As exhibited in Fig. 8a, TFC_W membranes presented a gradually reduced negatively charged surface from pH = 2 to pH = 10, which was mainly resulted from the dissociation of carboxyl acid groups.[2,39] Under the condition of pH = 7.0, the membrane potential was −12.83, −21.18, −25.50, −27.93 and −35.88 mV for $TFC_{W\text{-}0:1}$, $TFC_{W\text{-}1:0}$, $TFC_{W\text{-}4:1}$, $TFC_{W\text{-}1:4}$ and $TFC_{W\text{-}1:1}$ membrane, respectively. As evidenced in Fig. 7, $TFC_{W\text{-}1:1}$ possessed the highest content of the carboxyl acid groups when MPD/PIP mass ratio reached 1 : 1, thus it exhibited the lowest membrane potential compared to other TFC_W membranes. Notably, contents of O–C=O group not only induced the change of the membrane charge, but also had a great influence on the surface hydrophilicity, which was one of the most important factors determining the membrane permeability.

The surface hydrophilicity reflected by the measured contact angle values was displayed in Fig. 8b. For $TFC_{W\text{-}1:0}$ membrane, the contact angle was 53.45°. With the addition of PIP, all the TFC_W membranes showed lower contact angle than $TFC_{W\text{-}1:0}$ membrane but exhibited a decrease-increase change trend. When MPD and PIP mass ratio was 1 : 1, the membrane displayed the lowest contact angle. The interesting change was likely induced by comprehensive factors, including surface roughness, surface functional groups and surface charges.[40,41] Through the analysis of the surface chemical structure, moderate addition of PIP brought the increase of carboxyl group content and decline of membrane potential, which could contribute to the better hydrophilicity due to the affinity of membrane surface to water molecules. Since the $TFC_{W\text{-}1:1}$ membrane exhibited the lowest cross-linking degree, membrane potential and highest carboxyl group content, it contributed to the best hydrophilicity.

Separation performance of TFCW membranes

The separation performances of the TFC_W membranes were determined, including water flux and salt rejection. As seen in Fig. 9a, TFC_W membranes exhibited a gradually increased water flux as the increment of PIP concentration when using NaCl and Na_2SO_4 as the feed solution, and the form water flux (NaCl) was slightly higher than the latter (Na_2SO_4) one. In detail, the water permeability of $TFC_{W\text{-}1:0}$, $TFC_{W\text{-}4:1}$, $TFC_{W\text{-}2:1}$, $TFC_{W\text{-}1:1}$, $TFC_{W\text{-}1:2}$, $TFC_{W\text{-}1:4}$ and $TFC_{W\text{-}0:1}$ membrane for NaCl solution was 1.72, 2.23, 2.63, 2.93, 3.33, 3.73 and 4.23 L m^{-2} h bar, respectively. The flux enhancement was mainly ascribed to the improved

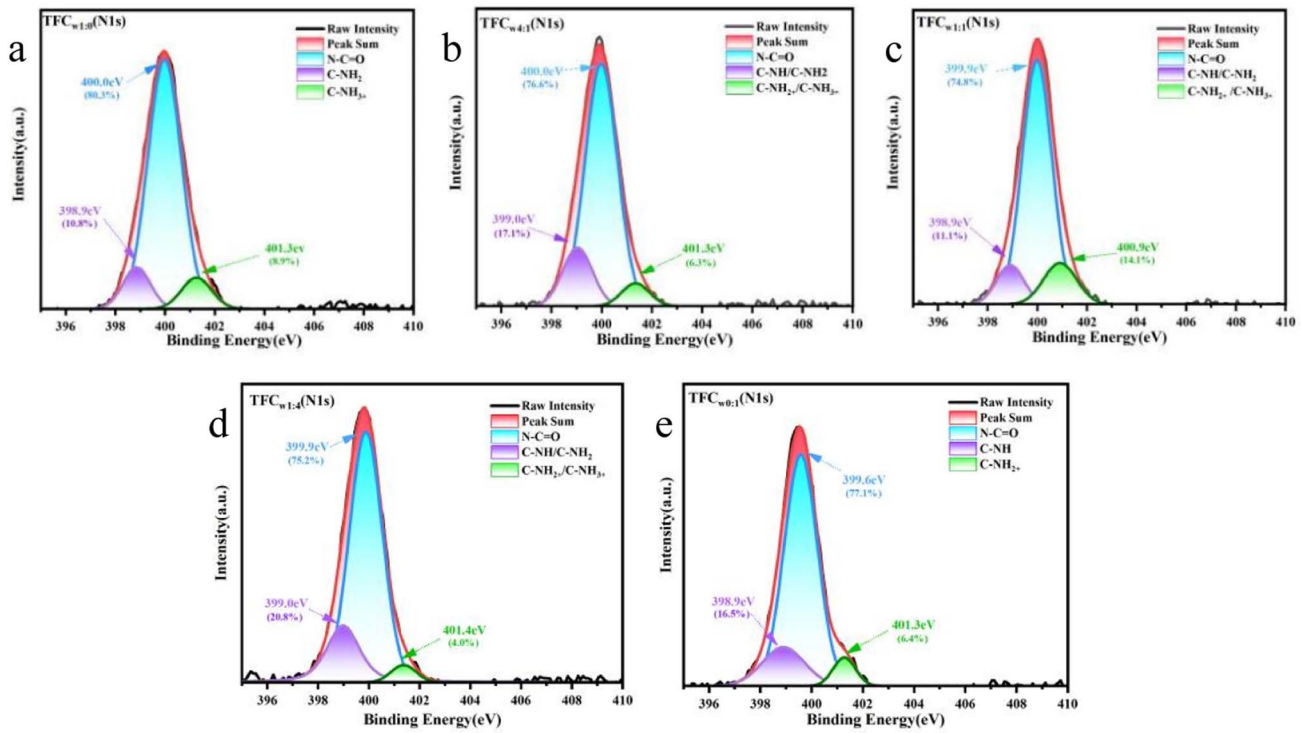

Fig. 7 N 1s deconvoluted peaks in XPS spectra.

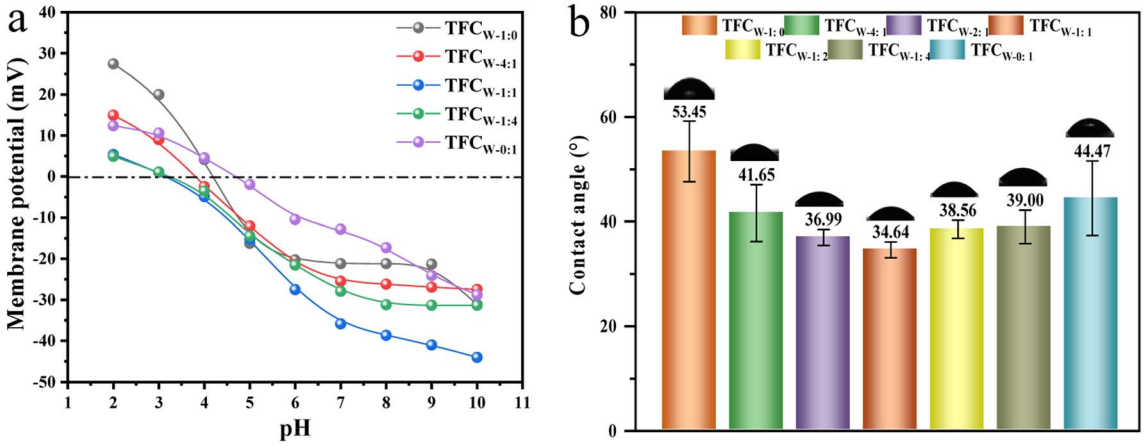

Fig. 8 (a) Membrane potential and contact angle (b) of TFC$_W$ membranes.

surface chemistry property and structure, such as membrane hydrophilicity, membrane potential and dense-degree of the PA layer. Fig. 9b and c calculated the flux enhancement rate of the TFC$_W$ membranes through the linear fitting of the water flux. It was clearly that both the flux enhancement rate increased from 6.477 to 6.838 for NaCl solution and from 5.693 to 8.693 for Na_2SO_4 solution when the PIP concentration surpassed 50%. As discussed above, as the incorporation of PIP in aqueous phase, it gradually participated in the formation of the initial PA layer. Specifically, when the concentration of PIP was below 50%, the initial PA layer was mainly controlled by the reaction between MPD and TMC, thus it still tended to form a dense layer with a gradually decreased dense degree with the addition of PIP. Consequently, a moderate enhanced water flux achieved. Nevertheless, once the concentration of PIP surpassed 50%, the reaction between PIP and TMC gradually dominated the IP

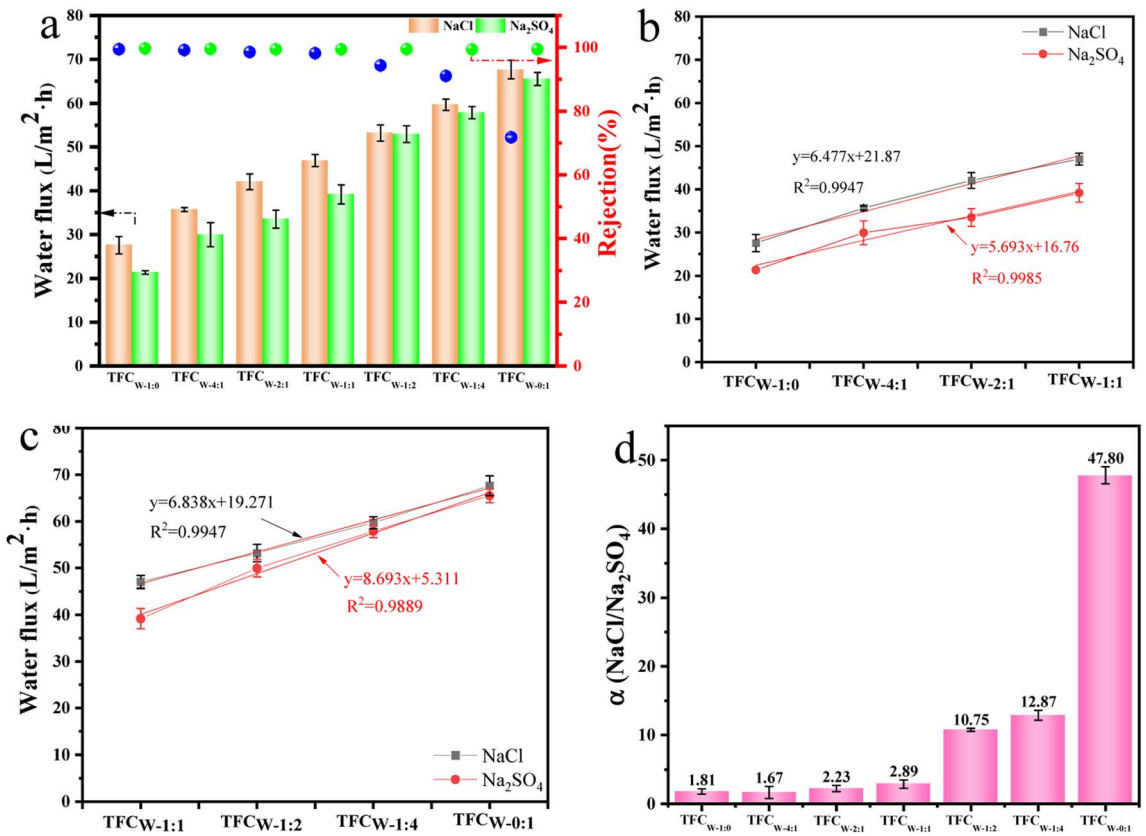

Fig. 9 (a) Separation of TFC$_W$ membranes for NaCl and Na_2SO_4, (b) and (c) flux enhancement rate of TFC$_W$ membranes with the PIP concentration below 50% and above 50% and (d) separation factor of NaCl to Na_2SO_4.

process, and induced a more loosen initial PA layer compared to MPD, which made a less resistant to water molecules to pass across the whole rejection layer. Thus, more obvious enhancement rate in water flux was observed.

From Fig. 9a, it can be also seen that the TFCw membranes exhibited greater rejection behaviors for Na_2SO_4 compared to NaCl, which were all extended by 99.3% and agreed well with the typical separation features for TFC-based RO and NF membranes. The higher rejection may result in a higher concentration of Na_2SO_4 compared to NaCl on the membrane surface and induce a more serious concentration polarization to weaken the effective driven force. Consequently, the water flux of Na_2SO_4 was slightly lower than that of NaCl. For monovalent salt, the rejection of NaCl was 99.4%, 99.1%, 98.5%, 98.1%, 94.3%, 90.9% and 71.8% for TFC_W membranes under the MPD/PIP mass ratio from 1 : 0 to 0 : 1, respectively. Obviously, the rejection of NaCl displayed a turning point at the MPD/PIP mass ratio about 1 : 1 with an unfavorable decline when further increasing the PIP concentration. This change would be also related to the different PA structures as discussed above.

The separation factor of NaCl to Na_2SO_4 was calculated based on their salt rejections, and the result was presented in Fig. 9d. The separation factor of NaCl to Na_2SO_4 increased from 1.81 to 47.79 with the increased loading concentration of PIP. Generally, the higher the separation coefficient, the better the selectivity of the membrane to monovalent and multivalent salts.[24] However, when systemic considering the water flux, NaCl rejection and separation factor of NaCl to Na_2SO_4, the best choice among all the TFC_W membranes was the $TFC_{W\text{-}1:1}$ membrane with a 70% flux enhancement accompanied by a 98.1% NaCl rejection and relatively higher separation efficiency of NaCl to Na_2SO_4. Table 3 compared the membranes fabricated in this study with other mixed-amine-based membranes, respectively. Of note, we roughly estimated the cost of preparing 100 mL of monomers for the aqueous phase based on previous references. It is observed that the membrane synthesized in this study has a higher performance in both flux and rejection than several other membranes. Only one membrane, the TAB-MPD membrane has a higher water flux, but it costs about 1.67 times higher to generate. In all, using PIP to regulate the performance of MPD-based RO membranes possessed great potential for commercial application.

Chlorine-resistant performance of TFCW membranes

NaCl rejection was the direct evidence in determining the chlorine-resistant capacity of TFC_W membranes when treated by 500 ppm NaClO solution. As shown in Fig. 10a, the TFC_W membranes exhibited different degradation degrees of the PA layer by active chlorine since all the membranes showed slight decline of NaCl rejection. Through the comparation between $TFC_{W\text{-}1:0}$ and $TFC_{W\text{-}1:1}$ membrane, both of them could maintain the integrity of PA layer after 12 h immersion in 500 ppm NaClO solution, since slight decrease of NaCl rejection for $TFC_{W\text{-}1:0}$ membranes changed from the 99.4% to 98.5% and 98.1% to 96.8% for $TFC_{W\text{-}1:1}$ membrane. However, when the immersion time was further extended to 24 h, obvious decline of NaCl rejection from 98.5% to 93.1% was detected for $TFC_{W\text{-}1:0}$ membranes, indicating an aggravated attack of active chlorine to PA layer, and 48 h immersion time induced more severe degradation. Consequently, the $TFC_{W\text{-}1:0}$ membrane displayed an 88.1% rejection to NaCl. On the contrary, $TFC_{W\text{-}1:1}$ membrane showed lower decline content of NaCl rejection after treatment of chlorin for 12 h and 48 h, and the final rejection was 94.3%, which was much higher than that of $TFC_{W\text{-}1:0}$ membrane. This change suggested the improved the chlorine resistant induced by the PIP addition in aqueous solution and delayed the degradation rate of PA layer. Fig. 10b displayed the Cl content detected by XPS in the membrane surface of the TFC_W membrane after 48 h immersion in 500 ppm NaClO solution. It was seen that $TFC_{W\text{-}1:1}$ membrane possessed the most content of Cl, which may be captured on the membrane surface in two ways, one was the attack of active chlorine to unreacted amine supplied by PIP and MPD molecules and the other one was the attack of active chlorine to amide bond followed by irreversible Orton rearrangement.

To further analyze the effect of PIP on the chlorine-resistant performance, the peak of Cl 2p was deconvoluted for four specific peaks at 197.1 eV (197.2 eV, 197.9 eV, 197.3 eV), 199.7 eV (199.8 eV, 199.1 eV, 200.0 eV), 200.2 eV (200.2 eV, 200.3 eV, 200.4 eV) and 201.7 eV (201.8 eV, 201.9 eV, 201.9 eV) as shown in Fig. 10c–f. Among them, the percentage of the two peaks at 200.6 eV and 202.2 eV represented C–Cl bond (organic Cl) was mainly caused by the attack of active chlorine to the amide bond.[46,47] Obviously, the addition of PIP gradually weakened this type of Cl attack. For $TFC_{W\text{-}1:0}$ membrane, the organic Cl occupied 87.0% of the total Cl, suggesting the severe deterioration of the fully aromatic PA separating layer and thus resulting in the visible decline of NaCl rejection. For $TFC_{W\text{-}1:1}$ membrane, 52.5% organic Cl reflected the decreased degradation of amide bond though it was unavoidably attacked by active chlorine. Shintani *et al.* measured the retention ratio of molecular weight (RRMW) after the immersion in chlorine

Table 3 Comparison of the performance and cost of current membranes with those of other mixed amine membranes

Membrane material	Optimal ratio	Water permeability (L m^{-2} h bar)	NaCl rejection (%)	Cost of 100 mL aqueous (¥)	Ref.
PIP-MPD	1 : 1	2.93	98.1	6.28	This work
TAB-MPD	0.3 : 1.7	11.10	97.7	10.5	42
DABS-MPD	0.1 : 1.9	0.25	92.1	10.23	43
BAPA-MPD	0.1 : 1.9	1.13	93.7	9.49	37
DABA-MPD	0.25 : 1.75	2.77	98.1	9.78	44
PAR-MPD	0.015 : 3.485	1.40	99.4	17.38	45

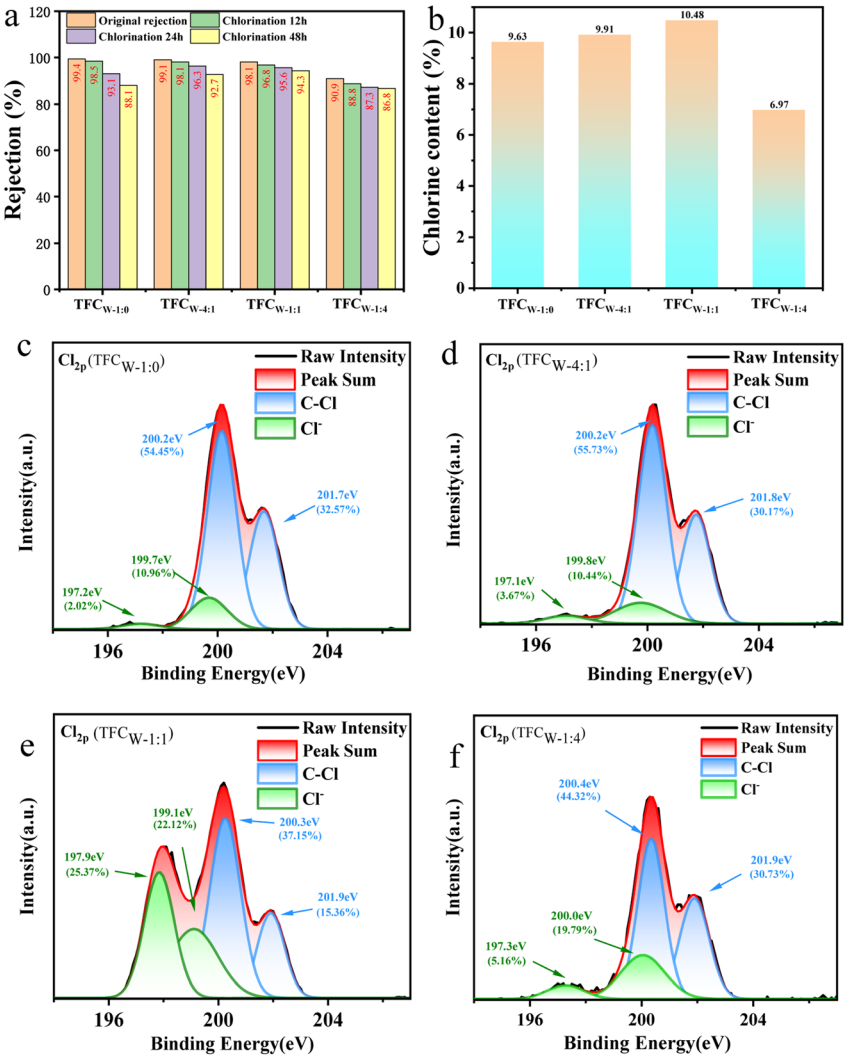

Fig. 10 (a) NaCl rejection of TFC_W membranes after immersion in 500 ppm NaClO solution, (b) chlorine content of TFC_W membranes after 48 h immersion detected by XPS, (c)–(f) Cl 2p deconvoluted peaks in XPS spectra.

solution as one of the evaluations of chlorine resistance. They found that the RRMW of PIP (0.65) was significantly higher than that of MPD (0.34), which may contribute to higher chemical resistance of amide bond and difficulty to break.[48] Besides, the highest content of unreacted amines of $TFC_{W\text{-}1:1}$ membrane provided abundant of binding site to consume active Cl, reflected by the increased content of Cl^- from 13.0% for $TFC_{W\text{-}1:0}$ membrane to 47.5% for $TFC_{W\text{-}1:1}$ membrane, and thus providing a protecting layer for amide bond from been direct attack.[22] Furthermore, it should be not ignored that addition of PIP increased the thickness of PA layer, and the extended PA layer was believed to serve as a sacrificial protective layer to maintain the integrity of the inner rejection layer. Resultingly, the $TFC_{W\text{-}1:1}$ membrane exhibited a slight decline of NaCl rejection after immersion for 48 h in NaClO solution. In light of the above analysis, addition of PIP in the aqueous solution played a positive role in enhancing the chlorine-resistant performance of TFC RO membranes.

Conclusion

In present study, the effect of PIP on the separation performance and chlorine-resistant of TFC RO membranes was evaluated. Addition of PIP in the aqueous solution interfered the IP process, such as lowering the diffusion rate of the mixed amine from the aqueous solution to the organic phase and lowering the reaction rate between amines and TMC. The PA layer of TFC RO transformed from 'fully-aromatic' PA structure to 'semi-aromatic' PA structure with the appearance of a ring structure on the membrane surface. When PIP and MPD mass ratio reached 1 : 1, the diffusion of amines molecule and reaction rate with TMC were both lower than other ratios. Besides, the $TFC_{W\text{-}1:1}$ membrane possessed the highest hydrophilicity and negative charged membrane potential, which contributed to 70% flux enhancement with 98.1% NaCl rejection and 99.4% Na_2SO_4 rejection. Of note, further increase of PIP concentration resulted in sharp decrease of NaCl rejection. Last but not least, PIP played a vital role in enhancing the chlorine-resistant of TFC RO

membranes, since the NaCl rejection of $TFC_{W\text{-}1:0}$ membrane declined from 99.4% to 88.1% (declined by 11.3%) and 98.1% to 94.3% for $TFC_{W\text{-}1:1}$ membrane (just declined by 3.8%) after immersion in 500 ppm NaClO solution for 48 h. Such improvement can be ascribed to the following two reasons, (1) the increased number of unreacted amine groups and thickness of PA layer that PIP brought could provide a sacrificial protective layer to consume the active chlorine, and thus maintain the integrity of the inner rejection layer; and (2) PIP-amide possessed no amidic hydrogen that caused higher difficulty to attack by active chlorine, and thus contributed to further improve of chlorine-resistant. MPD and PIP were the two commonly used amines to prepare commercial RO and NF TFC membranes. Experiments showed that it was an excellent choice to regulation of MPD-based IP process by using mature, cheaply and widely used PIP to improve the separation performance and chlorine-resistant, which possessed the most potential for the large-scale preparation of high-performance RO membranes.

Conflicts of interest

The authors declare that they have no known competing financial interests or personal relationships that could have appeared to influence the work reported in this paper.

Acknowledgements

This research was funded by the Natural Science Foundation of Shandong Province (ZR2022QE190), Chinese Postdoctoral Science Foundation (2020M672122).

References

1 Y. Liu, X. P. Wang, Z. A. Zong, R. Lin, X. Y. Zhang, F. S. Chen, W. D. Ding, L. L. Zhang, X. M. Meng and J. Hou, *J. Membr. Sci.*, 2022, **653**, 120520.
2 Q. Wang, J. Sun, W. Xue, G. Zhao, W. Ding, K. Zhang, S. Wang and Y. Li, *Desalination*, 2023, **546**, 116216.
3 Y. Zhang, Y. Wan, G. Pan, H. Yan, X. Yao, H. Shi, Y. Tang, X. Wei and Y. Liu, *Appl. Surf. Sci.*, 2018, **433**, 139–148.
4 Y. Zhao, X. Song, M. Huang, H. Jiang and A. Toghan, *Nano Res.*, 2022, **16**, 6153–6159.
5 D. L. Zhao, S. Japip, Y. Zhang, M. Weber, C. Maletzko and T. S. Chung, *Water Res.*, 2020, **173**, 115557.
6 K. P. Lee, T. C. Arnot and D. Mattia, *J. Membr. Sci.*, 2011, **370**, 1–22.
7 C. Yu, X. Cen, D. Ao, Z. Qiao and C. Zhong, *Appl. Surf. Sci.*, 2023, **614**, 156186.
8 Z. Wang, S. Liang, Y. Kang, W. Zhao, Y. Xia, J. Yang, H. Wang and X. Zhang, *Prog. Polym. Sci.*, 2021, **122**, 101450.
9 J. Farahbakhsh, V. Vatanpour, M. Khoshnam and M. Zargar, *React. Funct. Polym.*, 2021, **166**, 105015.
10 S. L. Li, P. Wu, J. Wang, J. Wang and Y. Hu, *Desalination*, 2020, **473**, 114169.
11 B. H. Jeong, E. M. V. Hoek, Y. Yan, A. Subramani, X. Huang, G. Hurwitz, A. K. Ghosh and A. Jawor, *J. Membr. Sci.*, 2007, **294**, 1–7.
12 H. Saleem and S. J. Zaidi, *Desalination*, 2020, **475**, 114171.
13 D. Li, H. Lu, X. Yan, H. Wan, G. Yan and G. Zhang, *J. Appl. Polym. Sci.*, 2022, **140**, e53518.
14 V. T. Do, C. Y. Tang, M. Reinhard and J. O. Leckie, *Environ. Sci. Technol.*, 2012, **46**, 852–859.
15 R. Verbeke, V. Gómez and I. F. J. Vankelecom, *Prog. Polym. Sci.*, 2017, **72**, 1–15.
16 S. Yu, M. Liu, Z. Lü, Y. Zhou and C. Gao, *J. Membr. Sci.*, 2009, **344**, 155–164.
17 F. Asempour, S. Akbari, M. H. Kanani-Jazi, A. Atashgar, T. Matsuura and B. Kruczek, *J. Membr. Sci.*, 2021, **623**, 119039.
18 H. R. Chae, J. Lee, C. H. Lee, I. C. Kim and P. K. Park, *J. Membr. Sci.*, 2015, **483**, 128–135.
19 Y. J. Tang, Z. L. Xu, S. M. Xue, Y. M. Wei and H. Yang, *J. Membr. Sci.*, 2016, **498**, 374–384.
20 W. Fang, L. Shi and R. Wang, *J. Membr. Sci.*, 2014, **468**, 52–61.
21 A. Pal, T. K. Dey, M. Sundararajan and R. C. Bindal, *ACS Appl. Polym. Mater.*, 2022, **4**, 2481–2496.
22 S. Liu, C. Wu, X. Hou, J. She, S. Liu, X. Lu, H. Zhang and S. Gray, *J. Membr. Sci.*, 2019, **573**, 36–45.
23 J. Li, X. Zhu, C. Lai, F. Chen, L. Bai, X. Cheng, J. Wang, D. Wu, J. Xu and H. Liang, *Desalination*, 2023, **545**, 116165.
24 X. Cheng, C. Lai, X. Zhu, S. Shao, J. Xu, F. Zhang, J. Song, D. Wu, H. Liang and X. Luo, *Desalination*, 2023, **548**, 116264.
25 W. Ding, H. Zhuo, M. Bao, Y. Li and J. Lu, *Chem. Eng. J.*, 2017, **330**, 337–344.
26 S. Xia, L. Yao, Y. Zhao, N. Li and Y. Zheng, *Chem. Eng. J.*, 2015, **280**, 720–727.
27 Y. Baek, H. J. Kim, S. H. Kim, J. C. Lee and J. Yoon, *J. Ind. Eng. Chem.*, 2017, **56**, 327–334.
28 P. Sarkar, S. Ray, B. Sutariya, J. C. Chaudhari and S. Karan, *Sep. Purif. Technol.*, 2021, **279**, 119692.
29 X. Cheng, C. Lai, J. Li, W. Zhou, X. Zhu, Z. Wang, J. Ding, X. Zhang, D. Wu, H. Liang and C. Zhao, *ACS Appl. Mater. Interfaces*, 2021, **13**, 57998–58010.
30 S. J. Park, S. J. Kwon, H. E. Kwon, M. G. Shin, S. H. Park, H. Park, Y. I. Park, S. E. Nam and J. H. Lee, *Polymer*, 2018, **144**, 159–167.
31 C. Y. Zhu, C. Liu, J. Yang, B. B. Guo, H. N. Li and Z. K. Xu, *J. Membr. Sci.*, 2021, **627**, 119142.
32 D. Xu, J. Zheng, X. Zhang, D. Lin, Q. Gao, X. Luo, X. Zhu, G. Li, H. Liang and B. Van der Bruggen, *Environ. Sci. Technol.*, 2022, **56**, 1927–1937.
33 W. Ding, Y. Li, M. Bao, J. Zhang, C. Zhang and J. Lu, *RSC Adv.*, 2017, **7**, 40311–40320.
34 X. Li, Z. Wang, X. Han, Y. Liu, C. Wang, F. Yan and J. Wang, *J. Membr. Sci.*, 2021, **640**, 119765.
35 Z. Zhang, G. Kang, H. Yu, Y. Jin and Y. Cao, *Desalination*, 2019, **466**, 16–23.
36 J. M. Gohil and P. Ray, *Sep. Purif. Technol.*, 2017, **181**, 159–182.
37 A. Waheed, U. Baig, A. Matin, S. M. S. Jillani, N. A. A. Qasem and I. H. Aljundi, *Desalination*, 2023, **549**, 116311.

38 P. Sarkar, S. Modak and S. Karan, *Adv. Funct. Mater.*, 2020, **31**, 2007054.
39 D. Xu, X. Zhu, X. Luo, Y. Guo, Y. Liu, L. Yang, X. Tang, G. Li and H. Liang, *Environ. Sci. Technol.*, 2021, **55**, 1270–1278.
40 C. G. Jothi Prakash, C. Clement Raj and R. Prasanth, *J. Colloid Interface Sci.*, 2017, **496**, 300–310.
41 Y. Xia, Z. Wang, L. Y. Chen, S. W. Xiong, P. Zhang, P. G. Fu and J. G. Gai, *Desalination*, 2020, **488**, 114510.
42 M. Kazemi, M. Jahanshahi and M. Peyravi, *Mater. Chem. Phys.*, 2020, **255**, 123592.
43 M. Yam-Cervantes, Y. Pérez-Padilla and M. Aguilar-Vega, *J. Appl. Polym. Sci.*, 2018, **135**, 46500.
44 H. Wang, L. Li, X. Zhang and S. Zhang, *J. Membr. Sci.*, 2010, **353**, 78–84.
45 L. Zhao, S. Liang, Y. Jin, Z. Wang, L. Hu, Y. Kang, J. Tao and W. Peng, *J. Appl. Polym. Sci.*, 2019, **505**, 144415.
46 S. Gholami, J. López, A. Rezvani, V. Vatanpour and J. L. Cortina, *Chem. Eng. J.*, 2020, **384**, 123348.
47 K. Hashiba, S. Nakai, M. Ohno, W. Nishijima, T. Gotoh and T. Iizawa, *Environ. Sci. Technol.*, 2019, **53**, 9109–9117.
48 T. Shintani, H. Matsuyama and N. Kurata, *Desalination*, 2007, **207**, 340–348.